Konya Mühendislik Bilimleri Dergisi, c. 12, s. 4, 955-970, 2024
Konya Journal of Engineering Sciences, v. 12, n. 4, 955-970, 2024
ISSN: 2667-8055 (Electronic)
DOI: 10.36306/konjes.1531085

DETERMINATION OF SOLAR REFLECTION COEFFICIENTS (ALBEDO) FROM SATELLITE IMAGES USING GOOGLE EARTH ENGINE PLATFORM

[1],* Mehmet Alper YILDIZ, [2] Hakan KARABÖRK, [3] Selmin ENER RÜŞEN

[1]Selçuk University, Kadınhanı Faik İçil Vocational School, Surveying Department, Konya, TÜRKİYE
[2] Konya Technical University, Natural and Applied Sciences Faculty, Geotechnical Engineering Department, Konya, TÜRKİYE
[3] Karamanoğlu Mehmetbey University, Director of Energy Efficiency Application & Research Center, Karaman, TÜRKİYE
[1] mayildiz@selcuk.edu.tr, [2] hkarabork@ktun.edu.tr, [3] selminerusen@kmu.edu.tr

Highlights

- For the summer and winter applications, the albedo value for snowy surfaces was calculated as 0.86, while for light-colored buildings, it was 0.36 for summer and 0.28 for winter.
- In conclusion, not only general surface albedo coefficients based on classes but also individually assigned surface albedo coefficients for each pixel have been created, enabling detailed and precise calculation of solar radiation values within the study area.
- This study diverges from global and local albedo calculations by converting high spatial resolution (10 meters) Sentinel 2A data using the Google Earth Engine Platform into albedo coefficients specific to the study area.

***Corresponding Author:** Mehmet Alper YILDIZ, mayildiz@selcuk.edu.tr

Konya Mühendislik Bilimleri Dergisi, c. 12, s. 4, 955-970, 2024
Konya Journal of Engineering Sciences, v. 12, n. 4, 955-970, 2024
ISSN: 2667-8055 (Electronic)
DOI: 10.36306/konjes.1531085

DETERMINATION OF SOLAR REFLECTION COEFFICIENTS (ALBEDO) FROM SATELLITE IMAGES USING GOOGLE EARTH ENGINE PLATFORM

[1],* Mehmet Alper YILDIZ, [2] Hakan KARABÖRK, [3] Selmin ENER RÜŞEN

[1]Selçuk University, Kadınhanı Faik İçil Vocational School, Surveying Department, Konya, TÜRKİYE
[2] Konya Technical University, Natural and Applied Sciences Faculty, Geotechnical Engineering Department, Konya, TÜRKİYE
[3] Karamanoğlu Mehmetbey University, Director of Energy Efficiency Application & Research Center, Karaman, TÜRKİYE
[1] mayildiz@selcuk.edu.tr, [2] hkarabork@ktun.edu.tr, [3] selminerusen@kmu.edu.tr

(Received: 12.08.2024; Accepted in Revised Form: 15.10.2024)

ABSTRACT: In many models calculating solar radiation, a combination of physical measurements and mathematical models is used to achieve results close to reality. In these calculations, the slope values and shading effects in the region being analyzed are often disregarded. Mathematical models such as ArcGIS's Area Solar Radiation (ASR) can calculate shading effects on three-dimensional surfaces. When solar radiation models are computed in three dimensions, accounting for solar rays reflected from the ground, in addition to atmospheric reflections, will increase accuracy.

This study aimed to determine the surface reflectance coefficients that should be added in three-dimensional radiation models. In literature, general assumptions exist for surface reflectance coefficients, which represent very broad average values. However, this study aimed to establish precise albedo values for all land classes and surfaces. An area of approximately 1600 km² located in the mountainous region south of Karaman was chosen as the test area. This area was chosen in Karaman province because, as is known, this region has high solar energy potential. Sentinel 2A satellite images with a spatial resolution of 10 meters were used for both summer and winter seasons through the Google Earth Engine (GEE) platform. For the summer and winter applications, the albedo value for snowy surfaces was calculated as 0.86, while for light-colored buildings, it was 0.36 for summer and 0.28 for winter. Although examples were provided for some land classes, the study ultimately determined albedo values for all land surfaces without differentiation between classes.

Keywords: *Solar Reflection Coefficients, Google Earth Engine Platform, Solar Panels, Solar Radiation*

1. INTRODUCTION

When solar radiation enters the Earth's atmosphere from space, a portion of the energy is reflected, scattered, absorbed, and scattered by atmospheric parameters [1]. Solar radiation that reaches the Earth's surface after being scattered by substances such as air, dust, aerosols, clouds, and water vapor in the atmosphere forms the concept known as diffuse solar radiation. The condition where solar radiation reaches the Earth's surface without undergoing any scattering is referred to as "Direct Solar Radiation" or "Beam Solar Radiation." [2, 3]. The total solar radiation reaching the Earth's surface, defined as "Global Solar Radiation" [4] is the sum of the diffuse and direct radiation components. To accurately determine Global Solar Radiation at the Earth's surface, numerous researchers have developed various measurement and estimation techniques. In solar radiation prediction models, three primary approaches stand out: statistical, physical, and hybrid models [5]. Physical models involve terrestrial measurements, such as global solar radiation, bright sunshine duration and air temperature etc. These terrestrial measurements are obtained ground measurements station challenging to deploy globally due to their costliness in maintenance and initial setup. Ground measurements instruments such as Pyranometers and Pyrheliometers are used in physical measurement methods to detect diffuse or direct solar radiation,

***Corresponding Author:** Mehmet Alper YILDIZ, mayildiz@selcuk.edu.tr

providing high accuracy. However, frequent field maintenance and high initial setup costs restrict their widespread use [3].

Another computational method is statistical techniques. In statistical methods, the prediction of solar radiation can be achieved using methods such as Long Short-Term Memory [6], Artificial Neural Network [7], Convolutional Neural Network [8, 9], and Gated Recurrent Units [10]. The accuracy of each method tends to vary according to regional and operational characteristics. A classical statistical model that achieves high performance in forecasting Global Solar is the Angström model [11], which utilizes surface measurements taken on a horizontal plane. Angström, established the first and simplest empirical relationship expressing the global solar radiation using computed measurements of sunshine duration and cloudless sky conditions [11]. Hybrid methods incorporate satellite-based techniques using meteorological satellites to obtain Solar Radiation information and maps. This estimation models are combine the high-precision data of ground observation stations and the ability of satellite data to cover large areas. These methods are widely used to generate Solar Radiation maps and data due to the relatively high spatial and temporal resolution capabilities of geographic weather satellites. Such advantages enable the widespread use of satellite imagery for predicting both Global and Diffuse Solar Radiation [12].

Accurate determination of the albedo value is an important parameter in all estimation methods, and it is directly included in formulas and calculations used to compute solar radiation. The concept of Albedo (Surface Reflectance Coefficient) refers to the rate at which solar radiation reaching the Earth's surface is reflected back by terrain surfaces or objects on the Earth's surface. Diffuse radiation caused by back reflection is important for all systems using solar energy. For example, solar panels can generate electricity not only from direct solar radiation but also from diffuse solar radiation. Therefore, albedo calculations are used in the calculation of systems directly related to solar radiation, such as heating systems and solar energy technologies [1]. Additionally, in next-generation bifacial photovoltaic solar panels, which enable two-way electricity generation, the albedo value is an important input [13, 14]. To increase the albedo coefficient and so electric generation, white stones or sand surfaces are created under the panels [15].

The Earth's albedo value is generally considered to range between 0.29 and 0.31 on average. This means that only about one-third of the solar radiation reaching the Earth's surface is reflected back into space. The remaining radiation is utilized for heating the Earth's surface and fulfilling various energy needs [16]. Functions such as plant photosynthesis, warming of seas and atmospheres, electricity generation, and energy requirements make use of the remaining solar radiation. However, it's crucial to note that the albedo value varies across different regions of the Earth. For instance, polar regions covered with ice have high albedo values, whereas dense and complex forests have low albedo values. One of the primary reasons for this variability is that the bright white color of snow cover reflects nearly 80-90% of the sunlight back to space. Similarly, desert areas and urban centers also represent regions with high albedo. Considering the different climate types and geographies worldwide, it becomes evident that each region and season exhibits varying albedo values and averages. Therefore, when calculating average albedo values, seasonal cycles and predominant land cover should also be taken into account [1].

Upon reviewing studies on albedo, it is observed that research predominantly focuses on calculating the albedo of specific surfaces [17, 18, 19, 20, 21]. Furthermore, various efforts have been made to generalize and compute averages for creating global albedo models [1, 22, 23, 24, 25]. However, this study diverges from global and local albedo calculations by converting high spatial resolution (10 meters) Sentinel 2A data using the Google Earth Engine Platform into albedo coefficients specific to the study area. The primary goal of this study is to establish albedo coefficients for each pixel across the entire study area, ensuring more precise values for solar radiation formulas applicable to every surface type. Different images from summer and winter were used to accurately calculate albedo values. The developed algorithms and formulas can be directly utilized in different regions to compute albedo values. Calculating albedo values for every pixel on Sentinel 2A images allows for accessing albedo coefficients for surfaces such as buildings, water bodies, soil, snow, mountains, forests, roads, rivers, and inclined surfaces in shade.

2. MATERIAL AND METHODS

2.1. Study Area

The study area was selected as a 1600 km² region located south of Konya province and north of Karaman province. The distinctive feature of this area is its representation of different topographic features and seasons, essential for calculating solar reflectance coefficients across all terrain and seasonal conditions. Reflectance coefficients typically reach their maximum on snowy surfaces. Therefore, the chosen study area represents a region with extensive snow cover during winter months. Additionally, the difference between inclined and horizontal radiation values is entirely due to the slope factor. Hence, careful attention was paid to selecting a study area with a diverse topography, including slopes. Furthermore, the presence of both flat and sloped areas in the study region is crucial for considering shading factors in calculating solar reflectance coefficients. Taking all these factors into account, the selected area encompasses all necessary variations in topographic features and seasonal changes. This ensures comprehensive evaluation and calculation of solar reflectance coefficients across different terrain types and seasonal variations. Figure 1 shows the study area boundaries on the map.

Figure 1. The study area boundaries

2.2. Spatial Datasets

Sentinel 2A satellite images with a resolution of 10 meters were used to classify the study area on the Google Earth Engine platform. Although Landsat images could also be used, their 30-meter resolution does not fully capture shading effects in areas with low slopes when calculating solar reflectance coefficients. Therefore, Sentinel 2A satellite images with their higher 10-meter resolution were chosen for this study.

As part of the Copernicus Programme of the European Commission (EC), the European Space Agency (ESA) has developed and is currently operating the Sentinel-2 mission. This mission acquires optical imagery at high spatial resolution (10 to 60 m) [26]. The Sentinel-2 mission has been enhanced to provide continuous monitoring services for global terrestrial and coastal surfaces. It offers systematic global

coverage of land and coastal areas, a high revisit frequency of five days under the same observation conditions, high spatial resolution, and a wide swath width (295 km) for multispectral observations across 13 bands in the visible, near-infrared, and shortwave infrared ranges of the electromagnetic spectrum. Sentinel-2 satellites systematically acquire observations over land and coastal areas from −56° to 84° latitude [27, 28]. A sample Sentinel 2A satellite imageries belongs to surface reflectance and top of atmosphere reflectance catalog are given in Figure 2.

Figure 2. Sentinel 2A surface reflectance and top of atmosphere reflectance imageries

2.3. Google Earth Engine Platform

Google Earth Engine is a cloud computing platform designed for processing satellite imagery and other geospatial and observational data. This platform provides users with access to satellite images and the computational power necessary to perform various analyses [20]. Introduced by Google in 2010, GEE has become the most popular and successful spatial analysis tool [45]. GEE provides access to a vast database of satellite imagery and the computational resources needed to analyze these [29, 30]. In recent years, GEE has been used in research on ecology [31] urban monitoring [32, 33] disaster management [34, 35, 36]and atmospheric studies [37].

2.4. Solar Radiation and Determination of Pixel Based Reflection Coefficients

The Earth receives a large amount of solar energy daily. The intensity of this radiation is influenced by various factors such as weather conditions, atmospheric distribution (including reflection, scattering, and absorption phenomena) [38]. Understanding solar radiation is crucial for calculating various performance metrics related to solar energy systems such as solar water heaters and photovoltaic systems. Global Solar Radiation incident on an inclined surface consists of three components: direct, diffuse, and reflected radiation values. Incoming solar radiation (insolation) from the sun is modified as it passes through the atmosphere, and further altered by topography and surface characteristics, resulting in distinct direct, diffuse, and reflected components. Direct solar radiation is the radiation received without obstruction directly from the sun. As for Diffuse solar radiation is scattered by atmospheric components like clouds and dust. Another one is Reflected solar radiation that is the radiation reflected by land classes and objects on the Earth's surface. The sum of direct, diffuse, and reflected solar radiation is termed total or global solar radiation. Generally, direct solar radiation is the largest component of total solar radiation, followed by diffuse solar radiation. Reflected solar radiation usually constitutes a small portion of total solar radiation, though this proportion can be higher in areas surrounded by highly reflective surfaces such as snow cover. Solar radiation calculation tools do not include reflected solar radiation in the calculation of total solar radiation. Therefore, total solar radiation is calculated as the sum of direct and diffuse solar radiation [39, 40, 41, 42, 44]. Diffuse, direct, and reflected solar radiations are simulated in Figure 3.

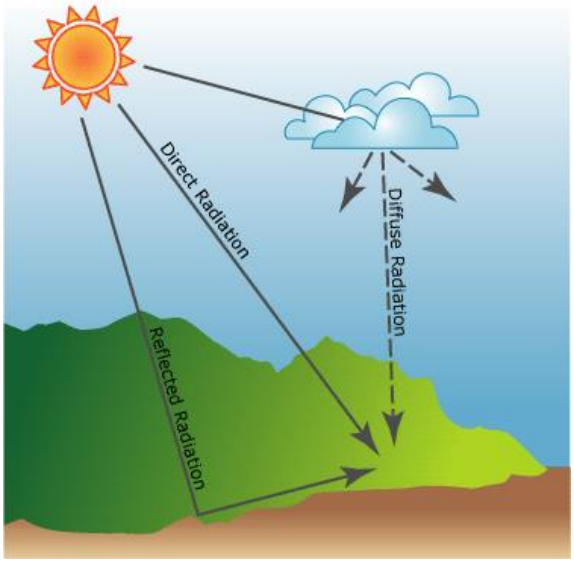

Figure 3. Diffuse, Direct and Reflected Solar Radiations [44]

The total solar radiation value at a point is calculated as the sum of the effects of different parameters and can be determined by the equation given in Formula 1.

$$q_s = I_b.cos\emptyset + H_d.cos^2\frac{\beta}{2} + H.p_s.sin^2\frac{\beta}{2} \quad (1)$$

In this formula, Ib represents the direct incoming solar radiation, while Hd parameterizes the diffuse solar radiation incident on a horizontal surface. H denotes the total global solar radiation at the specific point, ps signifies the surface reflectance coefficient, β indicates the surface slope angle, and $\emptyset$ represents the angle between the inclined surface and the solar beam. As seen in the formula, knowing the surface reflectance coefficient ps is essential for calculating the total solar radiation. Surface reflectance coefficients are generally calculated by the Italian National Agency for New Technologies, Energy and Sustainable Economic Development (ENEA) [46], which has computed average reflectance coefficients for various land classes. These values are averages and may vary depending on the study area and the surface characteristics of the land class.

The SRC determined by ENEA are shown in the Table 1. According to the table, fresh snow provides the highest reflectance, while roadways and water surfaces have very low reflectance values. However, upon examining the roadways in our country, they reflect dark gray, light gray, white, and light-yellow colors due to their structure. Therefore, using a single reflectance coefficient for a single roadway class would result in a very coarse and superficial calculation of total solar radiation. Similarly, grouping different building roof structures, surface colors, and sizes under a single reflectance coefficient would reduce the accuracy in calculating the total radiation obtained. Therefore, instead of a coarse classification, it is necessary to calculate pixel-based reflectance coefficient values for each land surface to achieve more accurate calculations of total solar radiation.

Table 1. Surface Reflectance Coefficients of Surfaces.

Surface	Average Reflection Value (ρ_s)
Snow	0.75
Water	0.07
Soil	0.14
Roads	0.04
Coniferous Forests (Winter)	0.07
Autumun Forest	0.26
Asphalt	0.10
Concrete Surface	0.22
Dead Leaves	0.30
Dry Grass	0.20
Green Grass	0.26
Bituminous Sand Roof	0.13
Stony Surfaces	0.20
Building Surface Red Brick	0.27
Building Surface Light Color	0.60

3. RESULTS

3.1. Definition of the Study Area Boundaries

In the GEE platform, the first step is to define the boundaries of the study area. This allows for identifying satellite images that fall within the specified boundaries. For this purpose, the corner coordinates of the area delineating the study area have been introduced to the platform in the WGS84 system. The relevant code for this is shown in Figure 4.

```
// Alan tanımlamaları
var alan = ee.Geometry.Polygon(
  [[[32.80083046596685, 37.19928722710696],
    [32.80083046596685, 36.801251493540725],
    [33.20084506662035, 36.801251493540725],
    [33.20084506662035, 37.19928722710696]]], null, false)
```

Figure 4. Definition of the study area boundaries in GEE

In the GEE platform, the satellite images relevant to the defined area are found using point-in-polygon analysis. This method involves checking if any part of the area intersects with satellite images. If there is an intersection, those satellite images are added to the list of images that can be used for further analysis.

3.2. Mosaic and Clip Processes of the Sentinel 2A Imageries

Since satellite images arrived in different parts following the definition of the study area, the images were merged (mosaic) to cover the entire study area and the areas outside the boundary were clipped. Level-2A images with atmospheric corrections were used when defining Sentinel-2A images. Images with cloud cover less than 10% were filtered from the Copernicus/S2_SR_Harmonized library. After defining the desired date information, a single satellite image covering the entire study area was obtained. The codes for all these operations are shown in Figure 5.

```
// Sentinel-2 Level-2A uyumlaştırılmış görüntülerini birleştirme ve kırpma işlemi
var s2Collection = ee.ImageCollection('COPERNICUS/S2_SR_HARMONIZED')
  .filterBounds(alan)
  .filterDate('2023-02-21','2023-02-23')
  .filterMetadata('CLOUDY_PIXEL_PERCENTAGE', 'less_than', 10);

// Görüntülerin detaylarını konsola yazdırma
s2Collection.toList(s2Collection.size()).map(function(image) {
  return ee.Image(image).get('system:index');
}).getInfo().forEach(function(index) {
  print('Görüntü detayları:', ee.Image(s2Collection.filter(ee.Filter.eq
  ('system:index', index)).first()));
});

var mosaicImage = s2Collection
  .sort('CLOUD_COVER')
  .mosaic()
  .clip(alan)
  .toFloat();
```

Figure 5. Code blocks for mosaic and clip

3.3. Determination of Solar Reflection Coefficients

When determining the reflectance coefficients, weight values used in the study by [43] and colleagues were employed. As mentioned, reflectance coefficients were calculated more accurately using the B2, B3, B4, B5, B6, B7, B8, B11, and B12 bands. The characteristics, spectral ranges, and weight values of the bands used are provided in Table 2. Upon examining the weight values, it is observed that the B2, B3, and B4 bands are most effective in calculating the reflectance coefficients.

Table 2. Weight values of the Sentinel 2A bands

Band Number	Band Name	Wavelength λ (μm)	Spectral Interval Δλ (μm)	Esun (W/m2)	ωbi (-)
B1	Aerosols	0.443	0.02	1893	-
B2	Blue	0.49	0.065	1927	0.1324
B3	Green	0.56	0.035	1846	0.1269
B4	Red	0.665	0.03	1528	0.1051
B5	Red Edge 1	0.705	0.015	1413	0.0971
B6	Red Edge 2	0.74	0.015	1294	0.0971
B7	Red Edge 3	0.783	0.02	1190	0.089
B8	NIR	0.842	0.115	1050	0.0818
B8a	Red Edge 4	0.865	0.02	970	0.0722
B9	Water vapor	0.945	0.02	831	-
B10	-	1.375	0.03	360	-
B11	SWIR 1	1.610	0.09	242	0.0167
B12	SWIR 2	2.190	0.18	3	0.0002

The code block created to determine the reflection coefficients is shown in Figure 6. Since the scale of the band weight values is 0.00001 and at the same time the global reflection coefficient values will take values on a scale ranging from 0 to 1, calculations were made by multiplying each band value by 10000. The resulting product by multiplying each band by its weight value and combining it with the fusion method will represent the reflection coefficient of each pixel.

```
// Albedo hesaplama fonksiyonu (Güncellenmiş)
function calculateAlbedo(image) {
  var blue = image.select('B2').multiply(0.1836).divide(10000);    // B2 bantı (Mavi)
  var green = image.select('B3').multiply(0.1759).divide(10000);   // B3 bantı (Yeşil)
  var red = image.select('B4').multiply(0.1456).divide(10000);     // B4 bantı (Kırmızı)
  var RedEdge1 = image.select('B5').multiply(0.1347).divide(10000); // B5 bantı (Kızılötesi 1)
  var RedEdge2 = image.select('B6').multiply(0.1233).divide(10000); // B6 bantı (Kızılötesi 2)
  var RedEdge3 = image.select('B7').multiply(0.1134).divide(10000); // B7 bantı (Kızılötesi 3)
  var nir = image.select('B8').multiply(0.1001).divide(10000);     // B8 bantı (Yakın Kızılötesi)
  var swir1 = image.select('B11').multiply(0.0231).divide(10000);   // B11 bantı (Kısa Dalga Kızılötesi 1)
  var swir2 = image.select('B12').multiply(0.0003).divide(10000);   // B12 bantı (Kısa Dalga Kızılötesi 2)

  var albedo = blue.add(green).add(red)
                   .add(RedEdge1).add(RedEdge2).add(RedEdge3)
                   .add(nir).add(swir1).add(swir2);

  return albedo.toFloat(); // 0-1 arası değer döndümek isteniyorsa return albedo.clamp(0, 1).toFloat(); uygulanır
}

// Albedo Değerleri hesaplanır ve görselleştirilir
var albedo = calculateAlbedo(mosaicImage);
```

Figure 6. Codes for the SRC calculation in GEE platform

The raster files created in the GEE platform were transferred to the ArcGIS program for analysis based on land cover classes. Initially, without any normalization process, the obtained values were examined. For the summer period, reflection coefficient values were calculated with a minimum of 0.002 and a maximum of 1.680, while for the winter period, values ranged from a minimum of 0.000 to a maximum of 1.720. The average reflection coefficient value for the summer season was calculated as 0.22, whereas for the winter season, it was calculated as 0.32. The surface reflection coefficient maps before normalization are provided in Figure 7.

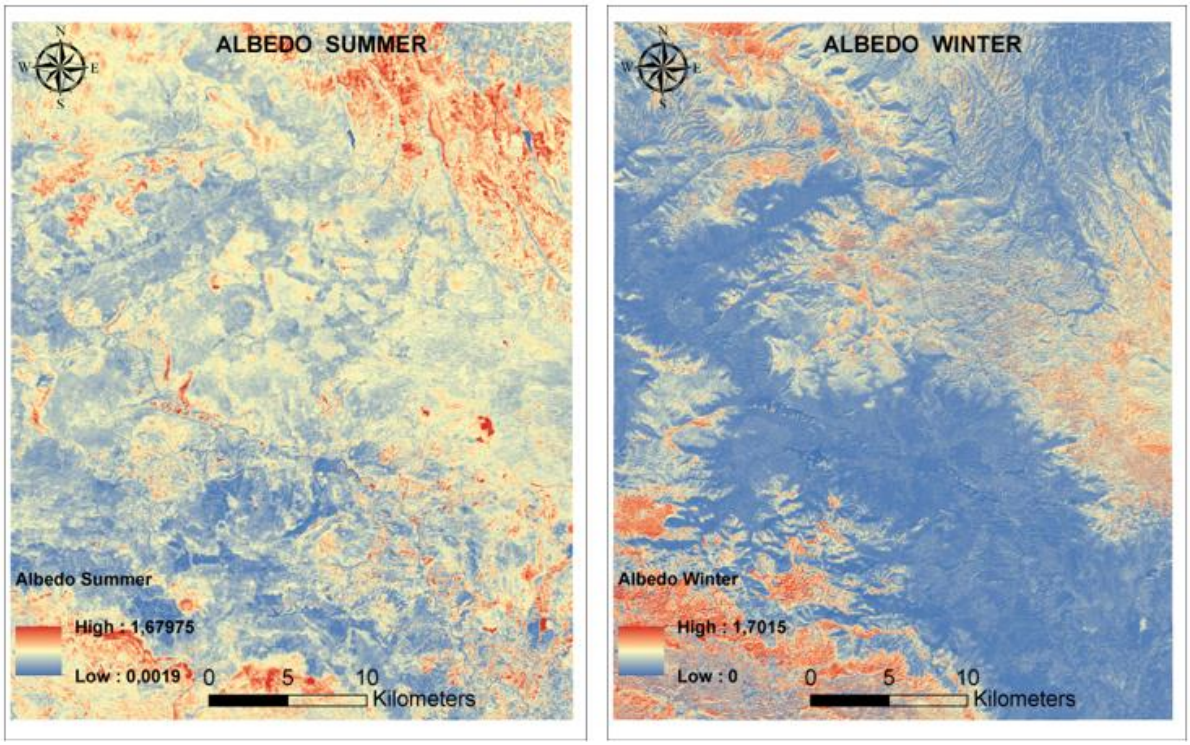

Figure 7. SRC rasters for winter and summer

According to the formulas created, the reflection coefficient values should range between 0 and 1. Here, a value of 0 represents no reflection at all, while a value of 1 indicates complete reflection. The raster values obtained from GEE have a maximum value exceeding 1. In reality, having regions with a reflection coefficient of exactly 0 might not be possible for the study area, whereas values exceeding 1 indicate that some pixels have excessively high reflection values. Upon examining the minimum and maximum values and reviewing the statistics of the result raster data, it was found that there are some pixels with undefined

or missing values. These empty values disrupt the 0-1 scale, causing some pixels to be calculated with higher values than expected. The aim is to classify each result raster data such that the maximum value does not exceed 1, identifying pixels with excessive values. Through this process, it was found that in the summer albedo maps, 43 pixels and in the winter albedo maps, 142718 pixels have values exceeding 1. The main reason for such high values in winter is the presence of extensive snow-covered surfaces. Given that each raster data consists of 20,000,000 pixels, the occurrence of pixels with values exceeding 1 represents approximately 0.007% for the winter season. The figure below shows the class intervals and the percentages of pixels with excessive values obtained for both summer and winter months. Class intervals and percentages of pixels with excessive values for summer and winter months are given in Figure 8.

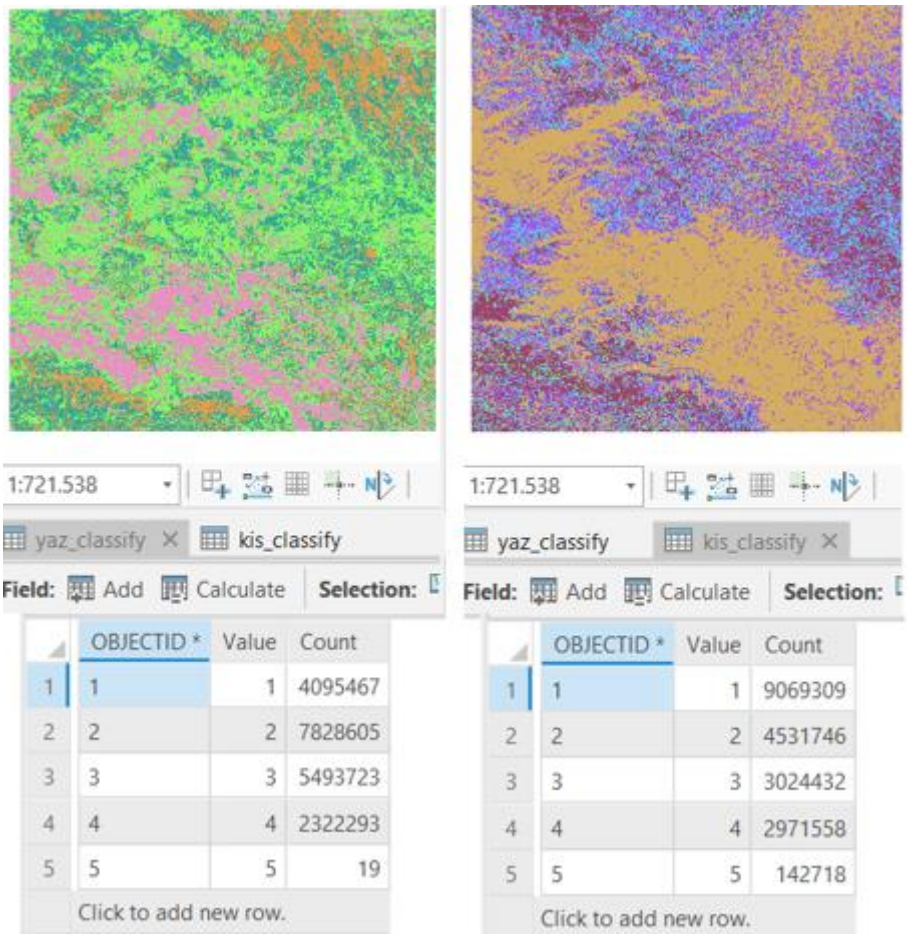

Figure 8. Unsampled pixels for winter and summer SRC rasters

In the generated Albedo rasters, there are values greater than 1 as well as pixels with no data. Using ArcGIS raster calculator, a resampling process was conducted for both pixels with no data and pixels with values greater than 1. This process consists of two main steps. First, all pixels greater than 1 were converted to nodata using the following code;

Con("Raster" > 1, SetNull("Raster", "Raster", "VALUE > 1"))

Subsequently, pixels that were set to nodata were resampled by taking values from neighboring pixels. Initially, it was planned to take values from the 8 neighboring pixels, but due to adjacent pixels with values greater than 1, the process failed. Therefore, an interpolation process was conducted using the neighborhood of 11 x 11 pixels. The following code block was used to assign values to each pixel by averaging the values of the surrounding 11 x 11 pixels.

FocalStatistics(Con("Raster" > 1, SetNull("Raster", "Raster"), "Raster"), NbrRectangle(11, 11, "CELL"),

"MEAN")

The surface albedo raster data for both summer and winter months have been generated as a result of all these processes. Each raster data has been obtained ensuring a minimum of 0 and a maximum of 1. The rasters are given in Figure 9.

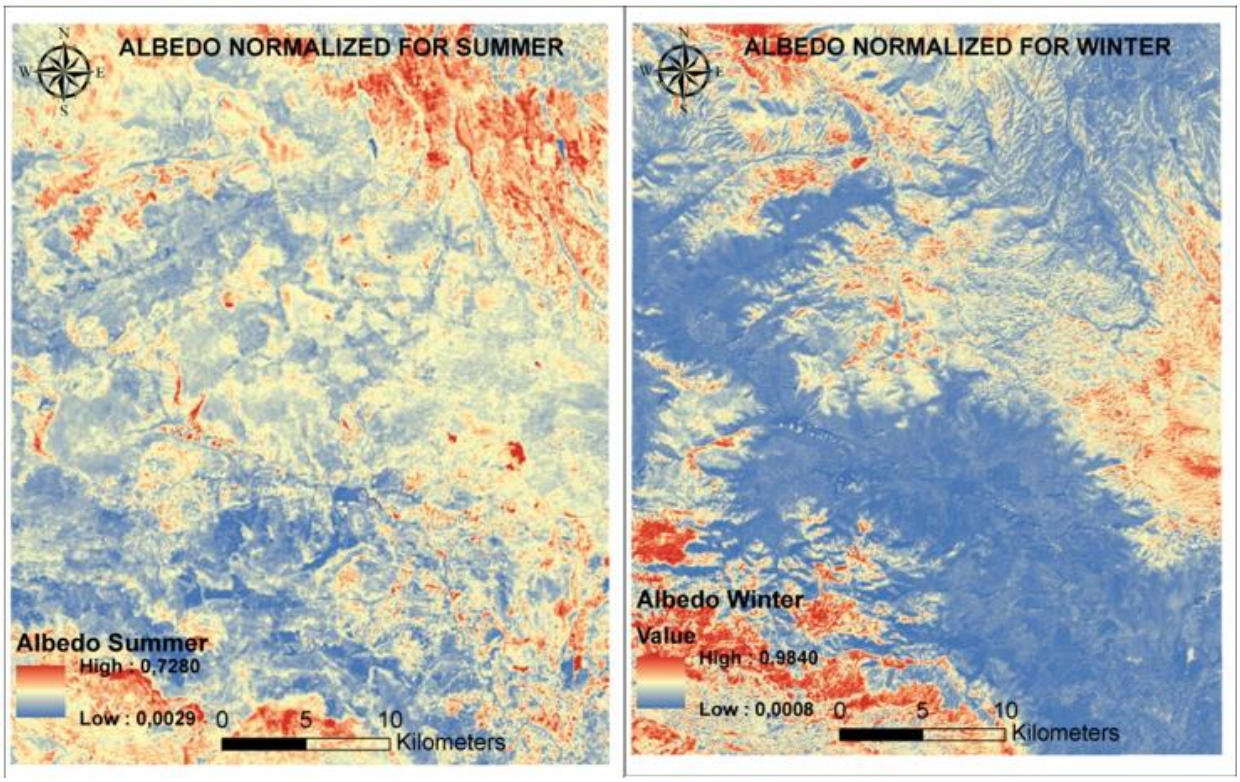

Figure 8. Normalized SRC rasters for winter and summer

The surface albedo coefficient values before and after resampling are provided in Table 3. It is observed that there is no change in the surface albedo coefficient value for the snow class. This is primarily because the highest surface albedo coefficient value corresponds to the snow surface class. After resampling, median changes were generally expected, for example, the light-colored building surface had a value of 0.55 before resampling and 0.36 after the process. Significant changes were not observed in other land use classes, generally showing tendencies towards similar values. In conclusion, not only general surface albedo coefficients based on classes but also individually assigned surface albedo coefficients for each pixel have been created, enabling detailed and precise calculation of solar radiation values within the study area.

Table 3. SRC values of all rasters

Surface	Before Resample		After Resample	
	Summer	Winter	Summer	Winter
Snow	-	0.86	-	0.85
Building Surface (Light color)	0.55	0.49	0.36	0.28
Building Surface (Red Brick)	0.27	0.22	0.27	0.23
Roads	0.22	0.23	0.20	0.19
Water	0.06	0.04	0.06	0.05

3.4. Converting Albedo to 3D Reflected Radiation Values

Three-dimensional solar radiation, due to shading caused by the terrain's topography, results in each face of the terrain having different sunlight durations and consequently varying solar radiation values. Therefore, considering the slope effect differently from horizontal solar radiation significantly contributes to the calculation of solar radiation. Using the ArcGIS Solar Radiation extension, direct and diffuse radiation values were generated with the help of the region's DEM map. Figure 9 shows the direct and diffuse radiation maps created for summer and winter months.

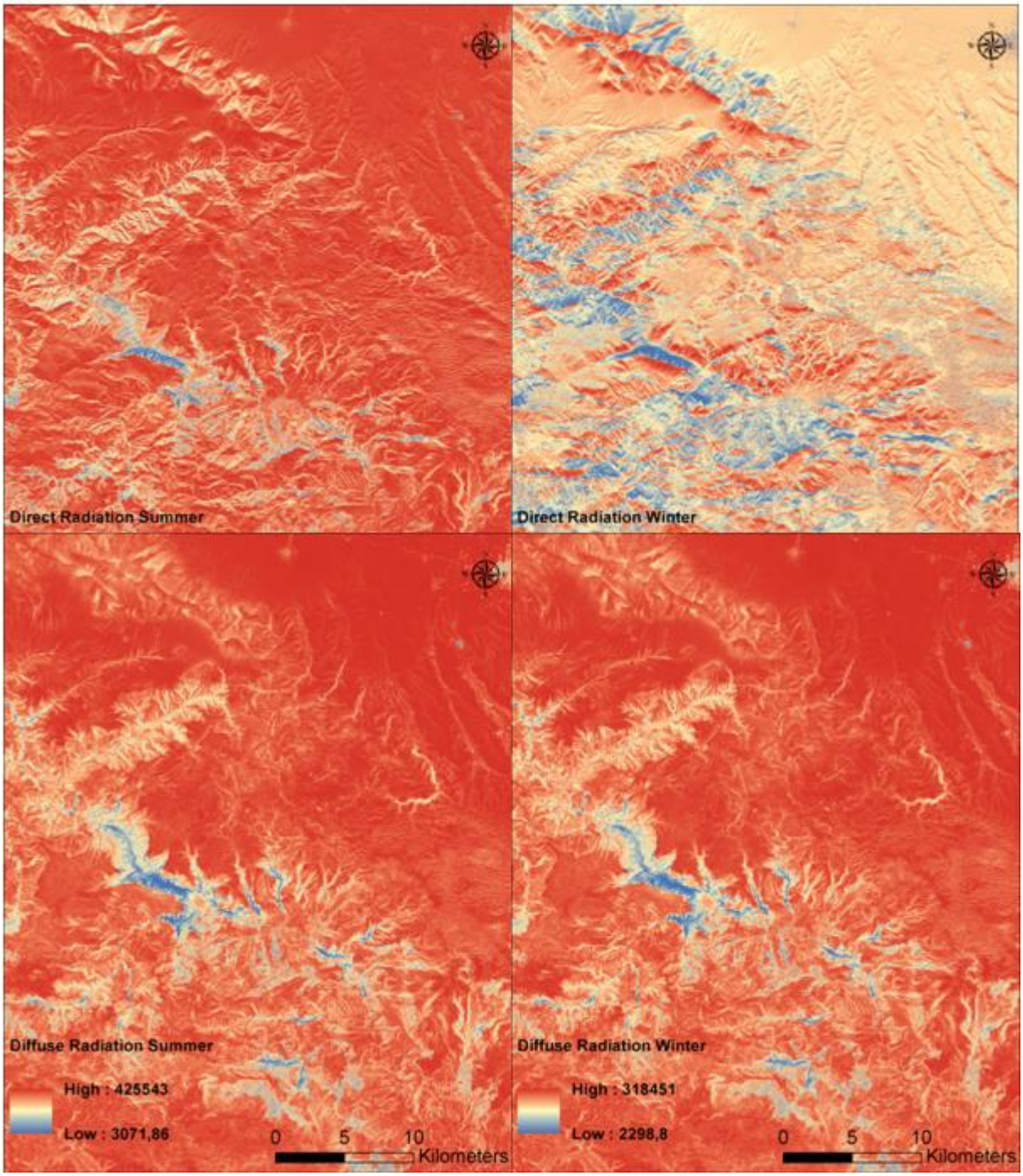

Figure 9. Diffuse and Direct radiation rasters for summer and winter

Reflected radiation values are affected by shading due to terrain features and slopes. Therefore, the

albedo evaluated horizontally may actually vary compared to the terrain surface. To address this variation, an inclination correction formula, Formula 2, has been applied to albedo values.

$$\text{Albedo} * (\sin(slope\ aim) * \frac{(\frac{\pi}{180})}{2})^2 * \text{Total Radiation} \quad (2)$$

In the formula, the slope angle values obtained from the DEM map were converted into slope percentages and multiplied with each pixel's albedo value. Thus, the albedo value adjusted for slope effect was calculated for each pixel. Since this adjusted value acts as a coefficient, multiplying it with the total radiation data yields the total solar radiation for three-dimensional surfaces. This approach provides more accurate and realistic solar radiation data for the region compared to global and horizontal radiation data. Figure 9 presents the total radiation values obtained using the calculated slope-adjusted albedo values for summer and winter months.

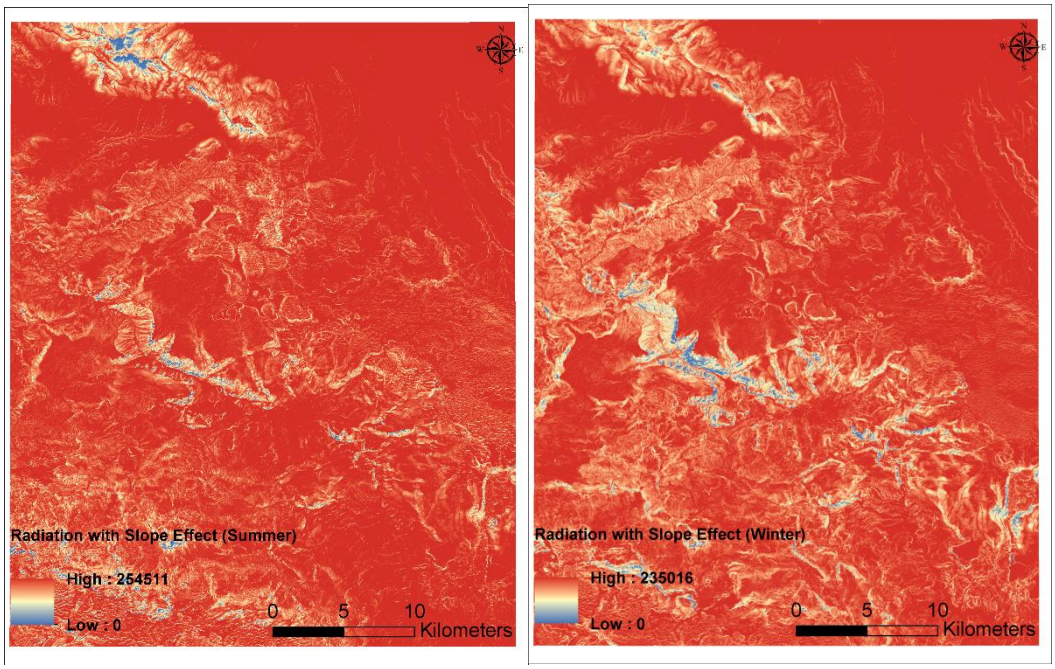

Figure 9. Radiation derived from albedo with slope

3. DISCUSSIONS

The purpose of this study is to reveal the maximum difference in albedo values between the summer and winter seasons. In studies conducted worldwide, albedo values are typically used as annual averages, generally derived from monthly averages. The duration of snow cover, the amount of snowfall during the season, and the number of cloudy and clear days are significant determining parameters for the annual and monthly average albedo values. This study investigates the effects of changes in albedo values on total radiation during the summer and winter months. Therefore, the focus is on the minimum and maximum values of albedo obtained for the region in both seasons, while overlooking the impacts of other such variables. To observe or eliminate the effects of these variables, long-term average albedo values need to be obtained. However, it will be crucial to derive these long-term average values of albedo when installing bifacial solar panels, which generate electricity from both sides, rather than conventional solar panels.

In this study, the total radiation values calculated using the ArcGIS Area Solar Radiation (ASR) module were utilized for computing albedo values. While performing calculations in the ASR module, 5-meter resolution digital elevation models were employed. The most critical factor in these calculations is

accounting for shading effects to provide accurate results. The calculation direction was chosen as 32, and the inclined radiation values for a 600x600 pixel area were calculated at every 11.25 degree angle over one year. Since the total radiation value obtained is used as a multiplier, the land topography was considered to derive the results. It was determined that a 5-meter DEM model is sufficient for the selected area. In cases where this study is conducted in populated areas, higher resolution imagery and DEMs would be necessary; however, the study conducted in non-populated areas is considered sufficient.

4. CONCLUSIONS

Accurate Albedo calculations hold significant importance in studies related to solar radiation. While global albedo values are currently used, and average albedo values for various land surfaces are known, these values may not provide sufficient accuracy for regional studies. Therefore, knowing continuous accurate albedo values specific to land surfaces is crucial. The widespread use of various solar energy applications where diffuse solar radiation values become important, such as bifacial solar panel designs, will significantly increase the effectiveness of accurate albedo values. In this context, the Google Earth Engine platform provides access to a vast amount and variety of satellite images, enabling rapid albedo calculations over large areas. Moreover, its high temporal resolution allows for the calculation of albedo values on a seasonal, monthly, and even weekly basis for regions, ensuring that albedo values are as close to reality as possible with minimized standard deviations. Additionally, with new satellite images continuously being uploaded to the GEE platform, dynamic and continuous calculation and observation of albedo values have become feasible. Since albedo values are generally included as an additional coefficient in solar radiation formulas, they contribute significantly to clarifying shading effects in 3D solar radiation calculations. Thus, integrating the albedo values obtained from this study into solar radiation calculations derived from any software or computation allows for more realistic and applicable solar radiation values to be calculated.

DECLARATION OF ETHICAL STANDARDS

This article does not require ethics committee permission

CREDIT AUTHORSHIP CONTRIBUTION STATEMENT

Formal analysis, validation, writing original draft, writing, review, and editing were performed by Hakan KARABÖRK and Selmin ENER RUSEN. Project administration and supervision were performed by Mehmet Alper YILDIZ. Conceptualization, data curation, investigation, methodology, resources, software, and visualization were performed by Mehmet Alper YILDIZ. All authors read and approved the final manuscript.

DECLARATION OF COMPETING INTEREST

The authors declare that they have no known competing financial interests or personal relationships that could have appeared to influence the work reported in this paper.

FUNDING / ACKNOWLEDGEMENTS

The author(s) received no financial support for the research, authorship, and/or publication of this article.

5. REFERENCES

[1] G. L. Stephens, D. O'Brien, P. J. Webster, P. Pilewski, S. Kato, and J. L. Li, The albedo of Earth,

Reviews of geophysics, 53(1), pp. 141-163, 2015.

[2] G. Gürsoy, Pv, rüzgâr türbini ve batarya içeren hibrid enerji sistemlerinde iyileştirilmiş optimal ölçeklendirme, Master's Thesis, Yıldız Technical University, Thesis Number. 406277, YÖK Thesis Center, 2015.

[3] M. Dursun, Küresel güneş radyasyonun makine öğrenmesi yöntemleri ile tahmini: örnek bir uygulama, Gaziantep İslam Bilim ve Teknoloji Üniversitesi Graduate School of Education, Department of Electrical and Electronics Engineering, Institute of Science, Master's thesis, 2023.

[4] Y. Özdemir, Uydu Tabanlı Kuadratik Model İle Türkiye'de Güneş Radyasyonu Dağılımının Belirlenmesi, Master's Thesis, Gazi University, Institute of Science, Ankara, 2012.

[5] S. Ener Ruşen, 2018. Performance Evaluation of a Coupled Method for the Estimation of Daily Global Solar Radiation on a Horizontal Surface, Atmósfera, 31, pp. 347-354, 2018.

[6] A. Kara, Global solar irradiance time series prediction using long short term memory network, *Gazi University Journal of Science Part C: Design and Technology,* 4, 7, 2019.

[7] G. Arslan, B. Bayhan and K. Yaman, Mersin/Türkiye için ölçülen global güneş ışınımının yapay sinir ağları ile tahmin edilmesi ve yaygın ışınım modelleri ile karşılaştırılması, *Gazi Üniversitesi Fen Bilimleri Dergisi Part C: Tasarım ve Teknoloji*,, pp. 7, 80-96, 2019.

[8] S. Ghimire, R. C. Deo, N. Raj and J. Mi, Deep solar radiation forecasting with convolutional neural network and long short-term memory network algorithms, *Applied Energy,* 253, 113541, 2019.

[9] B. Gao, X. Huang, J. Shi, Y. Tai and J. Zhang, Hourly forecasting of solar irradiance based on CEEMDAN and multi-strategy CNN-LSTM neural networks, *Renewable Energy,* 162, 1665-83, 2020.

[10] S. A. Haider , M. Sajid, H. Sajid, E. Uddin and Y. Ayaz, Deep learning and statistical methods for short-and long-term solar irradiance forecasting for Islamabad, *Renewable Energy*, 198, pp. 51-60, 2022.

[11] A. Angström, Solar and terrestrial radiation, Q. J. R. *Meteorolog. Soc.,* pp. 50,121–125, 1924.

[12] A. B. Karaveli, and B. G. Akınoğlu, Development of New Monthly Global and Diffuse Solar Irradiation Estimation Methodologies and Comparisons, *Int. J. Green Energy,* 15, pp. 325-346, 2018.

[13] A. Bayyiğit, O. K. Çinici, and A. Acır, Tek Yüzeyli ve Çift Yüzeyli Fotovoltaik Panellerin Performans Analizi. *Gazi University Journal of Science Part C: Design and Technology*, 11(2), pp. 407-420, 2023.

[14] X. Su, C. Luo, X. Chen and et al., Numerical modeling of all-day albedo variation for bifacial PV systems on rooftops and annual yield prediction in Beijing. *Build. Simul,* 17, pp. 955–964, 2024.

[15] M. H. Aksoy and M. K. Çalık, Performance Investigation of Bifacial Photovoltaic Panels at Different Ground Conditions, *KONJES,* vol. 10, no. 3, pp. 704–718, 2022.

[16] S. Bony and J. L. Dufresne, Marine boundary layer clouds at the heart of tropical cloud feedback uncertainties in climate models, *Geophys. Res. Lett.,* 32, L20806, 2005.

[17] J. Charney, W. J. Quirk, S. H. Chow and J. Kornfield, A comparative study of the effects of albedo change on drought in semi–arid regions, *Journal of the atmospheric sciences,* 34(9), 1366-1385. 1977.

[18] A. K. Betts and J. H. Ball, Albedo over the boreal forest. *Journal of Geophysical Research: Atmospheres,* 102(D24), 28901-28909, 1997.

[19] Z. Jin, T. P. Charlock, W. L. Smith Jr, and K. Rutledge, A parameterization of ocean surface albedo, *Geophysical research letters*, 31(22), 2004.

[20] A. S. Gardner, and M. J. Sharp, A review of snow and ice albedo and the development of a new physically based broadband albedo parameterization, *Journal of Geophysical Research: Earth Surface*, 115(F1), 2010.

[21] H. Akbari, H. D. Matthews and D. Seto, The long-term effect of increasing the albedo of urban areas. *Environmental Research Letters*, 7(2), 024004, 2012.

[22] J. R. Hummel, and R. A. Reck, A global surface albedo model, *Journal of Applied Meteorology and Climatology*, 18(3), pp. 239-253, 1979.

[23] A. Henderson-Sellers, and M. F. Wilson, Surface albedo data for climatic modeling, *Reviews of*

Geophysics, 21(8), , pp. 1743-1778, 1983.

[24] A. Hall, The role of surface albedo feedback in climate, *Journal of climate,* 17(7), pp. 1550-156, 2004.

[25] A. Donohoe and D. S. Battisti, Atmospheric and surface contributions to planetary albedo. *Journal of Climate*, 24(16), pp. 4402-4418, 2011.

[26] M. Drusch, U. Del Bello, S. Carlier, O. Colin, V. Fernandez F. Gascon, B. Hoersch, C. Isola, P. Laberinti, P. Martimort and et al. Sentinel-2: ESA's Optical High-Resolution Mission for GMES Operational Services, *Remote Sens. Environ*. 120, pp. 25–36, 2012.

[27] F. Gascon, C. Bouzinac, O. Thépaut, M. Jung, B. Francesconi, J. Louis, V. Lonjou, B. Lafrance, S. Massera, A. Gaudel-Vacaresse and et al. Copernicus Sentinel-2A Calibration and Products Validation Status, *Remote Sens.,* 9, 584, 2017.

[28] C. Revel, V. Lonjou, S. Marcq, C. Desjardins, B. Fougnie, C. Coppolani-Delle Luche, C. and X. Lenot, Sentinel-2A and 2B absolute calibration monitoring, *European Journal of Remote Sensing*, 52(1), pp. 122–137, 2019.

[29] L. Yu, P. Gong, Google Earth as a virtual globe tool for Earth science applications at the global scale: Progress and perspectives, *Int. J. Remote Sens*., 33, pp. 3966–3986, 2012.

[30] Q. Zhao, L. Yu, X. Li, D. Peng, Y. Zhang and P. Gong, Progress and Trends in the Application of Google Earth and Google Earth Engine, *Remote Sens.,* 13, 3778, 2021.

[31] T. Tao, S. Abades, S. Teng, Z. Y. X. Huang, L. Reino, B. J. W. Chen, Y. Zhang, C. Xu and J. C. Svenning, Macroecological factors shape local-scale spatial patterns in agriculturalist settlements, *Proc. R. Soc. B Biol. Sci*., 284, 2017.

[32] H. Du, W. Cai, Y. Xu, Z. Wang, Y. Wang and Y. Cai, Quantifying the cool island effects of urban green spaces using remote sensing Data, *Urban For. Urban Green*,27, pp. 24–31, 2017.

[33] A. Schneider, Monitoring land cover change in urban and pen-urban areas using dense time stacks of Landsat satellite data and a data mining approach, *Remote Sens. Environ*, 124, pp.689–704, 2012.

[34] M. Akbar, S. Aliabadi, R. Patel and M. Watts, A fully automated and integrated multi-scale forecasting scheme for emergency preparedness. *Environmental Modelling & Software*, 39, pp- 24–38, 2013.

[35] F. Giselle Murillo-Garcia, I. Alcantara-Ayala, F. Ardizzone, M. Cardinali, F. Fiourucci and F. Guzzetti, Satellite stereoscopic pair images of very high resolution: A step forward for the development of landslide inventories, *Landslides,* 12, pp. 277–291, 2015.

[36] J. Zhang, D. R. Gurung, R. Liu, M. S. R. Murthy and F. Su, Abe Barek landslide and landslide susceptibility assessment in Badakhshan Province, Afghanistan. *Landslides,* 12, pp. 597–609, 2015.

[37] A. Sharma, J. Wang and E. M. Lennartson, Intercomparison of MODIS and VIIRS fire products in Khanty-Mansiysk Russia: Implications for characterizing gas flaring from space, *Atmosphere*, 8, 95, 2017.

[38] A. Hall, and X. Qu, Using the current seasonal cycle to constrain snow albedo feedback in future climate change, *Geophys. Res. Lett.,* 33, L03502, doi:10.1029/2005GL025127, 2006.

[39] B. Y. Liu, and R. C. Jordan, The interrelationship and characteristic distribution of direct, diffuse and total solar radiation, *Solar energy,* 4(3), pp.1-19, 1960.

[40] D. Vernez, A. Milon, L. Vuilleumier, and J. L. Bulliard, Anatomical exposure patterns of skin to sunlight: relative contributions of direct, diffuse and reflected ultraviolet radiation, *British Journal of Dermatology*, 167(2), pp. 383-390, 2012.

[41] A. Höpe, Diffuse reflectance and transmittance, In Experimental Methods in the Physical Sciences , Vol. 46, *Academic Press,* pp. 179-219, 2014.

[42] S. Vanino and et al., Capability of Sentinel-2 data for estimating maximum evapotranspiration and irrigation requirements for tomato crop in Central Italy, *Remote Sensing of Environment* 215, , pp. 452–470, 2018.

[43] D. J. Wojcicki, Derivation of the effective beam radiation incidence angle equations for diffuse and reflected solar radiation using a two dimensional approach, *Solar Energy,* 112, pp. 272-281, 2015.

[44] ArcGIS Solar Radiation Documents. [Online]. Available:

https://desktop.arcgis.com/en/arcmap/latest/tools/spatial-analyst-toolbox/modeling-solar-radiation.htm [Accessed Apr.10, 2024].

[45] Wikipedia [Online]. Available: https://en.wikipedia.org/wiki/Google_Earth [Accessed Feb. 5, 2024].

[46] ENEA, Italian National Agency for New Technologies, Energy and Sustainable Economic Development [Online]. Available: https://www.enea.it/en/ [Accessed Feb. 10, 2024].